IEEE Access
Multidisciplinary | Rapid Review | Open Access Journal

Received May 15, 2019, accepted May 30, 2019, date of publication June 10, 2019, date of current version June 25, 2019.

Digital Object Identifier 10.1109/ACCESS.2019.2921968

Two-Stage Switching Hybrid Control Method Based on Improved PSO for Planar Three-Link Under-Actuated Manipulator

XIN GAO, ZEYU REN, LIN ZHAI, QINGXUAN JIA, (Member, IEEE), AND HUIHE LIU
School of Automation, Beijing University of Posts and Telecommunications, Beijing 100876, China

Corresponding author: Xin Gao (xlhhh74@bupt.edu.cn)

This work was supported in part by the Key Project of Chinese National Programs for Fundamental Research and Development (973 program), under Grant 2013CB733000 and the National Natural Science Foundation of China, under Grant 61573066.

ABSTRACT The planar three-link passive-active-active (PAA) under-actuated manipulator does not satisfy the small-time local controllability (STLC), which makes it more difficult to control than other planar under-actuated manipulators. This paper presents a two-stage switching hybrid control method based on improved particle swarm optimization (PSO) for the PAA under-actuated manipulator. According to the model reduction strategy, the control process is divided into two stages. The workspace of the manipulator is analyzed to guarantee the target position within the reachable region. In order to reduce the probability of falling into local optimum, we introduce the Metropolis criterion of simulated annealing algorithm and crowding factor of artificial fish swarm algorithm into PSO algorithm to calculate the target angles of two active joints. At each control stage, we design the Lyapunov function to maintain the angle of an active joint unchanged while we build the sliding surface and select the power function as reaching law to make the other active joint converge to the target angle. The control law switches to next stage when the rotated joint converges to the target angle. The proposed method not only retains the rapidity of sliding mode control, but also reduces the total chattering of the system by the Lyapunov function method. Simulation results demonstrate that the proposed method has shorter steady-state adjustment time than that of existing typical control methods, and its overshoot is almost zero.

INDEX TERMS The planar three-link passive-active-active (PAA) under-actuated manipulator, the improved particle swarm optimization (PSO), hybrid control method, Lyapunov direct method, sliding mode control.

I. INTRODUCTION

The under-actuated manipulator is a typical kind of nonlinear systems whose number of control inputs is less than that of degrees of freedom [1]. Compared with the full-actuated manipulator, the under-actuated manipulator has lighter weight and consumes less energy. Furthermore, the broken actuator of a normal manipulator may be difficult to be repaired in some applications especially in the space station or the nuclear radiation area. A suitable under-actuated control method can be adopted as an emergency control strategy to complete the tasks. Thus, the research on the control method of under-actuated manipulator has not only theoretical and practical significance, but also has wide application prospects. On account of the nonholonomic constraints, the control of the under-actuated manipulator is much more difficult than that of the full-actuated manipulator. Researchers have achieved some positive results in recent years [2]–[5]. There are two types of the under-actuated manipulator: the vertical manipulator, which is subject to gravity, and the planar manipulator, which is not. Due to the lack of gravity term, the general smooth feedback control method is ineffective for the planar under-actuated manipulator [6]. The research on the control method of the planar under-actuated manipulator can further improve the research theory in the under-actuated system and has important theoretical value.

The planar under-actuated manipulator can be divided into two types: the manipulator with the passive first

The associate editor coordinating the review of this manuscript and approving it for publication was Ning Sun.

joint and the manipulator with the passive non-first joint. Luca *et al.* [7] presented the small-time local controllability (STLC) and proved the controllability of the planar two-link under-actuated manipulator with the passive second joint (AP). Oriolo *et al.* [8] studied on integrability of the planar under-actuated manipulator and proved the complete integrability of the planar two-link under-actuated manipulator with the passive first joint (PA). In other words, the planar PA manipulator is controllable. BANAVAR *et al.* [9] researched on the controllability of planar three-link under-actuated manipulator with two active joints. They proved that the PAA manipulator does not satisfy STLC, which increases difficulty in control. Lai *et al.* [10] presented a model reduction strategy to solve the problem. According to the strategy, the PAA manipulator is transformed into two controllable planar PA manipulators.

Based on the model reduction strategy, the Lyapunov function is built to derive the control law for the two planar PA manipulators in [11]. While this method can design stable control law, there is no suitable method to design the optimal Lyapunov function at present [12]. The position control of the planar PAA manipulator is realized based on sliding mode control method in [13]. The manipulator is divided into several subsystems. Then, the sliding surface and switching item are designed for each subsystem, respectively. The total sliding surface is built based on the subsystems to stabilize the whole system. However, the sliding mode control method arises chattering problem and its performance on stability is not good.

The position control of the manipulator need to calculate the target angles of each joint. Its essence is to solve the inverse kinematics. Due to the complex model of the manipulator and the angle constraint among joints, the intelligent optimization algorithms are more suitable for the inverse kinematics [14]. Genetic algorithm (GA) which attempts to simulate the phenomenon of natural evolution is a kind of strong global stochastic search and parallel computation methods [15]. But the local searching capability of GA is weak. Simulated annealing algorithm is a kind of stochastic search methods which is inspired by the annealing process of solid materials in thermodynamics [16]. It shows good local optimization characteristics, but converges slow. Ant colony algorithm, which is known as good robustness and global optimization characteristics, solves optimization problems by positive feedback mechanism [17]. However, the algorithm is prone to stagnation phenomenon. Particle swarm optimization (PSO) algorithm which simulates the social behavior of bird flocking is a kind of global optimization methods [18]. Compared with other optimization algorithms, PSO converges faster and needs setting less parameters.

The inverse kinematics of the PAA under-actuated manipulator is solved by PSO [11]. The algorithm updates particles only depending on individual historical optimal particle and global optimal particle. But the algorithm is more likely to converge early and gets stuck in local optimum [19]–[21]. A hybrid optimization algorithm combining GA with PSO solved inverse kinematics for the planar PAA under-actuated manipulator in [22]. This method has strong global search ability, but its local search ability is still comparable to that performed in GA.

The paper presents a two-stage switching hybrid control method based on improved particle swarm optimization for the planar PAA under-actuated manipulator. The primary contributions of this paper are as follows:

1. In order to avoid premature convergence, we introduce the Metropolis criterion of simulated annealing algorithm into updating process to make it accept poorer solutions in a certain probability. In addition, in order to jump out of the local optimum and maintain the population diversity, we introduce the crowding factor of artificial fish swarm algorithm into PSO to control the movement direction of particles.

2. On the basis of obtaining the target angles of each joint, we present a two-stage switching hybrid control method. At each control stage, we design Lyapunov function to maintain the angle of an active joint unchanged while we build the sliding surface and select the power function as reaching law to make the other active joint converge to the target angle. The control law will switch to next stage when the rotated joint converges to the target angle. The proposed method not only retains the rapidity of sliding mode control, but also reduces the total chattering of the system by Lyapunov function method.

The paper is organized as follows: In section II, the control process is divided into two stages according to model reduction method and the workspace of the manipulator is analyzed. In section III, we present the improved PSO to solve the inverse kinematics of the planar PAA under-actuated manipulator. In section IV, the control law is designed by the proposed two-stage switching hybrid control method. Results of the simulation are illustrated in section V and the conclusions are made in section VI.

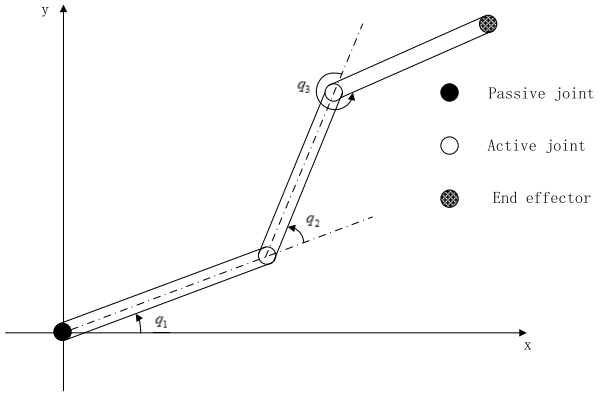

FIGURE 1. The planar three-link PAA under-actuated manipulator.

II. SYSTEM MODELING

A. KINEMATICS MODEL

Fig 1 shows the structure of a general planar three-link manipulator with the passive first joint. The research object in this

paper is the planar manipulator, so the gravity matrix term is not considered.

The parameters are as follows: q_i and L_i represent the joint angle and the length of the ith link, respectively.

According to the geometric constraint between the end effector position and the three joint angles, the kinematics model is given as follows:

$$\begin{cases} X = \cos(q_1)L_1 + \cos(q_1+q_2)L_2 + \cos(q_1+q_2+q_3)L_3 \\ Y = \sin(q_1)L_1 + \sin(q_1+q_2)L_2 + \sin(q_1+q_2+q_3)L_3, \end{cases} \tag{1}$$

where (X, Y) indicates the actual coordinates of the end effector.

B. DYNAMIC MODEL

The dynamic model (2) of the planar PAA under-actuated manipulator is built by Lagrange method [23].

$$M(q)\ddot{q} + H(q, \dot{q}) = \tau, \tag{2}$$

where $\dot{q}$ and $\ddot{q}$ represent the angular velocity and the angular acceleration, respectively. τ represents the input torque, $M(q) \in R^{3\times3}$ is the inertia matrix, and $H(q, \dot{q}) \in R^{3\times1}$ describes the Coriolis and centrifugal forces.

The dynamic model (2) can be transformed as follows:

$$\begin{bmatrix} M_{11} & M_{12} & M_{13} \\ M_{21} & M_{22} & M_{23} \\ M_{31} & M_{32} & M_{33} \end{bmatrix} \begin{bmatrix} \ddot{q}_1 \\ \ddot{q}_2 \\ \ddot{q}_3 \end{bmatrix} + \begin{bmatrix} H_1 \\ H_2 \\ H_3 \end{bmatrix} = \begin{bmatrix} 0 \\ \tau_2 \\ \tau_3 \end{bmatrix} \tag{3}$$

According to the dynamic equation (3), the constraint on the passive joint can be expressed as

$$M_{11}\ddot{q}_1 + M_{12}\ddot{q}_2 + M_{13}\ddot{q}_3 + H_1 = 0. \tag{4}$$

The planar PAA under-actuated manipulator is a nonholonomic system with no input term for the passive joint. The equation (4) is partially integrable [10]. Thus, we can obtain the constraints between the passive joint and each active joint. Then the passive joint can converge to the target angle through rotation of the active joints.

Base on model reduction strategy in [10], the control process is divided into two stages. In the first stage, the third joint is maintained in its initial angle and the second joint is controlled to the target angle. In second stage, the second joint is maintained in its angle and the third joint is controlled to the target angle.

C. ANALYSIS OF THE WORKSPACE

The workspace of the planar PAA under-actuated manipulator refers to the set of all positions that the end effector can reach. Based on model reduction strategy, we select many sets of joint angles calculating the end effector position to obtain the workspace. The simulation is conducted by MATLAB and the parameters are as follows: the length of each link is $l_1 = 0.8, l_2 = 1.2, l_3 = 1.0(m)$, respectively. The range of each joint angle is $[0, 2\pi]$ and the step size is set to 0.1rad. We traverse the angles of active joints to calculate the angle of the passive joint. Then, the position of end effector is calculated to obtain the workspace. Fig 2 shows the workspace of the planar PAA under-actuated manipulator.

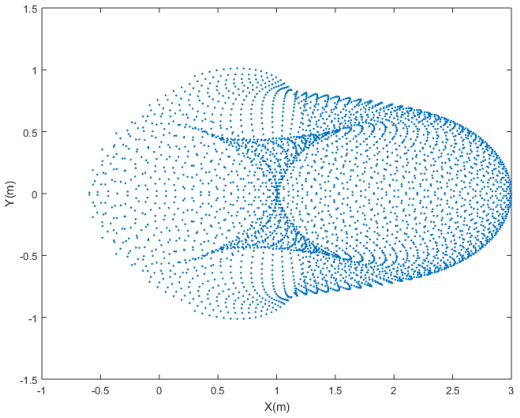

FIGURE 2. The workspace of the planar PAA under-actuated manipulator.

Fig 2 illustrates the workspace of the manipulator is not a complete circle. Since the passive joint is only driven by the active joints, the workspace is symmetrical about $x = 0$. The forward motion (Clock wise) is symmetrical about the reverse motion (Counter Clock wise). The end effector positions are densely distributed in $x \in [0, 3]$ and $y \in [-0.8, 0.8]$. The angles corresponding to adjacent points are similar. Therefore, the target angles need calculating accurately.

III. DESIGN OF IMPROVED PSO

The calculation of the target angles for each joint is essentially to solve inverse kinematics. The actual position of the end effector is related to the two active joint angles. The position error of the end effector is positive proportional to the error of each joint angle. In this section, the particle swarm optimization algorithm is selected to solve the inverse kinematics. In order to reduce the probability of falling into local optimum, we introduce the Metropolis criterion of simulated annealing algorithm [24] and crowding factor of artificial fish swarm algorithm [25] into PSO algorithm to calculate the target angles of two active joints. The proposed algorithm reduces the errors caused by the inaccurate joint angles and provides the optimal target angles for the position control.

The distance between the actual end effector position and the target position is chosen as the evaluation function of the optimization algorithm. The evaluation function is given as follows:

$$f = \sqrt{(X - X_d)^2 + (Y - Y_d)^2}, \tag{5}$$

where X_d, Y_d indicate the target coordinates of the end effector.

A. THE IMPROVED PSO

The procedures of the improved PSO are as follows:

Step 1: Initialization. The position of each particle is defined within the feasible domain. All particles obey uniform distribution and the speed of each particle is generated randomly within the feasible domain.

Step 2: The fitness of each particle is calculated according to equation (5) and we obtain the best individual position *Pbest* of each particle. Then, the global best position *Gbest* of the particle swarm is obtained.

Step 3: The Metropolis criterion of simulated annealing algorithm is introduced into PSO. Compared the fitness of each particle with *Pbest*, if the fitness is less than *Pbest*, *Pbest* will be replaced by this fitness. If not, a random number is generated from (0, 1) as reference. Compared the number with the acceptance probability p, if the number is bigger, *Pbest* will be replaced by the fitness.

The acceptance probability p is defined as

$$p = e^{5*(count\_best-count)/count\_best}, \tag{6}$$

where *count* is the number of current iterations, and *count_best* is the number of iterations corresponding to the personal optimal particle.

Step 4: Compared the fitness of each particle with *Gbest*, if the fitness is less than *Gbest*, *Gbest* will be replaced by this fitness.

Step 5: Each particle in the swarm updates itself according to equation (7) and (8):

$$V_i^{count+1} = \omega V_i^{count} + c_1 * rand * (Gbest - X_i) + c_2 * rand * (Pbest - X_i), \tag{7}$$

$$X_i^{count+1} = X_i^{count} + V_i^{count}, \tag{8}$$

where V_i^{count} and X_i^{count} are the speed and the position of the ith particle in the $count$th iteration, ω is the inertia weight, and c_1 and c_2 are weighting factors.

Step 6: The crowding factor of artificial fish swarm algorithm is introduced into PSO to avoid excessive concentration of the particles. When most of the particles are concentrated near to the global best position, we assume the particle swarm algorithm falls into local optimum. The distance d between the average position of the current particles and the global best position is calculated. If the distance d is less than the threshold δ, the global best position will be replaced by the average position to adjust the move direction of next generation particles. In this way, we increase the diversity of the particles and the proposed algorithm is more likely to jump out of local optimum.

Step 7: The algorithm is terminated when it reaches the maximum number of the iterations or the fitness meets the requirement, otherwise it returns to step 2.

B. ANALYSIS OF THE IMPROVED PSO

In this part, experiments are conducted to verify the superiority of the improved PSO compared with the other three algorithms. The parameters for each algorithm are shown in Table 1.

The initial state of the manipulator and the target position of the end effector are as follows:

$$q_{10} = q_{20} = q_{30} = 0,$$
$$\dot{q}_{10} = \dot{q}_{20} = \dot{q}_{30} = 0(rad/s),$$
$$(X_d, Y_d) = (2.6428, 0.1728).$$

TABLE 1. The parameters for each algorithm.

Parameters	GA	PSO	SPSO	The improved PSO
Population size(N)	300	300	300	300
Dimension	2	2	2	2
Inertia wight(ω)	_	0.53	0.53	0.53
Cognitive acceleration constant(c_1)	_	2	2	2
Social acceleration constant(c_1)	_	1.8	1.8	1.8
Threshold(δ)	_	_	_	0.1
Crossover probability	0.8	_	_	_
Mutation probability	0.05	_	_	_

TABLE 2. Simulation results.

	Average	Variance	Minimum	Maximum
GA	$7.15 * 10^{-6}$	$3.27 * 10^{-11}$	$1.61 * 10^{-6}$	$2.23 * 10^{-6}$
PSO	$8.95 * 10^{-5}$	$4.01 * 10^{-7}$	0	$4.48 * 10^{-3}$
SPSO	$1.83 * 10^{-3}$	$1.40 * 10^{-6}$	$1.74 * 10^{-4}$	$4.34 * 10^{-3}$
The improved PSO	$6.00 * 10^{-6}$	$1.79 * 10^{-9}$	0	$3.00 * 10^{-4}$

The experiments were repeated 50 times, and the average, variance, minimum and maximum of f are compiled in Table 2.

The average value of the evaluation function f of GA, PSO, SPSO, and the improved PSO are 7.15×10^{-6}, 8.95×10^{-5}, 1.83×10^{-3} and 6.00×10^{-6}, respectively. The improved PSO outperforms other three algorithms on the value of average and minimum, which means the algorithm is more likely to obtain the optimal target angles. Meanwhile, the improved PSO also performs well on the value of variance and maximum, which illustrates the algorithm has good stability.

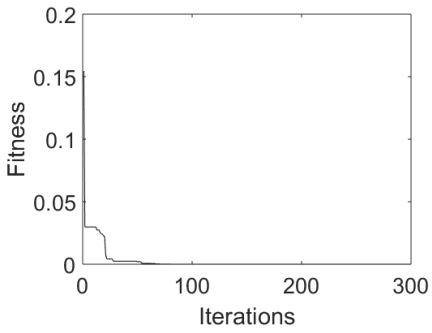

FIGURE 3. The fitness curve of the improved PSO algorithm.

The optimal target angles calculated by the improved particle swarm optimization algorithm are $q_{2d} = -1rad$, $q_{3d} = 1rad$. The fitness curve of the improved PSO algorithm is shown in Fig 3. The algorithm converges quickly in the first 50 iterations, then falls into local optimum and converges slow. The position of the global best particle is adjusted to make the algorithm jump out of local optimum. Then, the algorithm continues converging. The optimal target angles can be obtained at about $70th$ iterations.

IV. CONTROLLERS DESIGN

On the basis of obtaining the target angles of each joint, the control law is designed by the two-stage switching hybrid

control method. At each control stage, we design Lyapunov function to maintain the angle of an active joint unchanged while we build the sliding surface and select the power function as reaching law to make the other active joint converge to the target angle. The control law switches to next stage when the rotated joint converges to the target angle.

If we let $[x_1 \quad x_2 \quad x_3 \quad x_4 \quad x_5 \quad x_6]^T = [q_1 \quad \dot{q}_1 \quad q_2 \quad \dot{q}_2 \quad q_3 \quad \dot{q}_3]^T$, the dynamic model (3) of the planar PAA under-actuated manipulator can be written in state-space form as

$$\begin{cases} \dot{x}_1 = x_2 \\ \dot{x}_2 = F_1(x) + b_1(x)\tau_2 + c_1(x)\tau_3 \\ \dot{x}_3 = x_4 \\ \dot{x}_4 = F_2(x) + b_2(x)\tau_2 + c_2(x)\tau_3 \\ \dot{x}_5 = x_6 \\ \dot{x}_6 = F_3(x) + b_3(x)\tau_2 + c_3(x)\tau_3, \end{cases} \tag{9}$$

where τ_2 and τ_3 represent the input torque on the second joint and the third joint, respectively. The column vector, which consists of F_1, F_2 and F_3, satisfies

$$\begin{bmatrix} F_1 & F_2 & F_3 \end{bmatrix}^T = -M^{-1}(q)H(q, \dot{q}),$$

and the nonlinear functions $b_1(x)$, $b_2(x)$, $b_3(x)$, $c_1(x)$, $c_2(x)$ and $c_3(x)$ satisfy

$$\begin{bmatrix} b_1(x) & c_1(x) \\ b_2(x) & c_2(x) \\ b_3(x) & c_3(x) \end{bmatrix} = -M^{-1}(q) \begin{bmatrix} 0 & 0 \\ 1 & 0 \\ 0 & 1 \end{bmatrix}.$$

A. DESIGN OF FIRST-STAGE CONTROLLER

In the first stage, we design Lyapunov function to maintain the angle of the third joint unchanged while we build the sliding surface and select the power function as reaching law to make the second joint converge to the target angle. The steps are as follows:

Step 1: The Lyapunov function $V_1(x)$ is chosen as

$$V_1(x) = \frac{1}{2}(x_5 - x_5(0))^2 + \frac{1}{2}{x_6}^2, \tag{10}$$

$$\dot{V}_1(x) = x_6(x_5 - x_5(0) + F_3(x) + b_3(x)\tau_2 + c_3(x)\tau_3). \tag{11}$$

The designed control law needs to meet the condition $V_1(x) \geq 0, \dot{V}_1(x) \leq 0$ to guarantee the third joint angle unchanged. By considering $\dot{V}_1(x) = 0$, the constraint between τ_2 and τ_3 is given as follows:

$$\tau_3 = -\frac{x_5 - x_5(0) + F_3(x) + b_3(x)\tau_2}{c_3(x)}. \tag{12}$$

Step 2: The sliding surface is defined as $S_1{=}c_1x_3{+}x_4$, where c_1 is a positive constant.

Step 3: According to Filippov equivalent control theory in [26], the control law for the second joint can be defined as

$$\dot{S}_1 = c_1x_4 + F_2(x) + b_2(x)\tau_2 + c_2(x)\tau_3 = 0, \tag{13}$$

$$\tau_{eq_1} = -\frac{c_1x_4 + F_2(x) + c_2(x)\tau_3}{b_2(x)}. \tag{14}$$

Step 4: The switching item of sliding mode control is designed as follows:

$$\tau_{sw1} = -\frac{w_1|S_1|^{\alpha_1}sgn(S_1)}{b_2(x)}, \tag{15}$$

where α_1 is a constant in (0, 1).

Then, the control law for the second joint can be obtained using

$$\tau_2 = \tau_{eq_1} + \tau_{sw1.} \tag{16}$$

Substituting equation (16) into equation (12), we can obtain the control law in the first stage

$$\begin{cases} \tau_2 = (c_3(x)[c_1x_4 + F_2(x) + w_1|S_1|^{\alpha_1}sgn(S_1)] \\ \qquad -c_2(x)[x_5 - x_5(0) + F_3(x)]) \\ \qquad /(b_3(x)c_2(x) - b_2(x)c_3(x)) \\ \tau_3 = -(x_5 - x_5(0) + F_3(x) + b_2(x)\tau_2)/c_3(x). \end{cases} \tag{17}$$

Remark 1: τ_2 is proportional to the parameter w_1 and the steady-state adjustment time is inversely proportional to the parameter w_1. The parameter α_1 affects the smooth of the torque curve. If α_1 is selected too small, it will lead to oscillations of the torque curve.

B. DESIGN OF SECOND-STAGE CONTROLLER

In the second stage, we design Lyapunov function to maintain the angle of the second joint unchanged while we build the sliding surface and select the power function as reaching law to make the third joint converge to the target angle. The steps are as follows:

Step 1: The Lyapunov function $V_2(x)$ is chosen as

$$V_2(x) = \frac{1}{2}(x_3 - x_3(0))^2 + \frac{1}{2}{x_4}^2, \tag{18}$$

$$\dot{V}_2(x) = x_4(x_3 - x_3(0) + F_2(x) + b_2(x)\tau_2 + c_2(x)\tau_3). \tag{19}$$

The designed control law needs to meet the condition $V_2(x) \geq 0, \dot{V}_2(x) \leq 0$ to guarantee the second joint angle unchanged. By considering $\dot{V}_2(x) = 0$, the constraint between τ_2 and τ_3 is given as follows:

$$\tau_2 = -\frac{x_3 - x_3(0) + F_2(x) + c_2(x)\tau_3}{b_2(x)}. \tag{20}$$

Step 2: The sliding surface is defined as $S_2{=}c_2x_5{+}x_6$, where c_2 is a positive constant.

Step 3: According to Filippov equivalent control theory, the control law for the second joint can be defined as

$$\dot{S}_2 = c_2x_6 + F_3(x) + b_3(x)\tau_2 + c_3(x)\tau_3 = 0, \tag{21}$$

$$\tau_{eq_2} = -\frac{c_2x_6 + F_3(x) + b_3(x)\tau_2}{c_3(x)}. \tag{22}$$

Step 4: The switching item of sliding mode control is designed as follows:

$$\tau_{sw2} = -\frac{w_2|S_2|^{\alpha_2}sgn(S_2)}{c_3(x)}, \tag{23}$$

where α_2 is a constant in (0, 1).

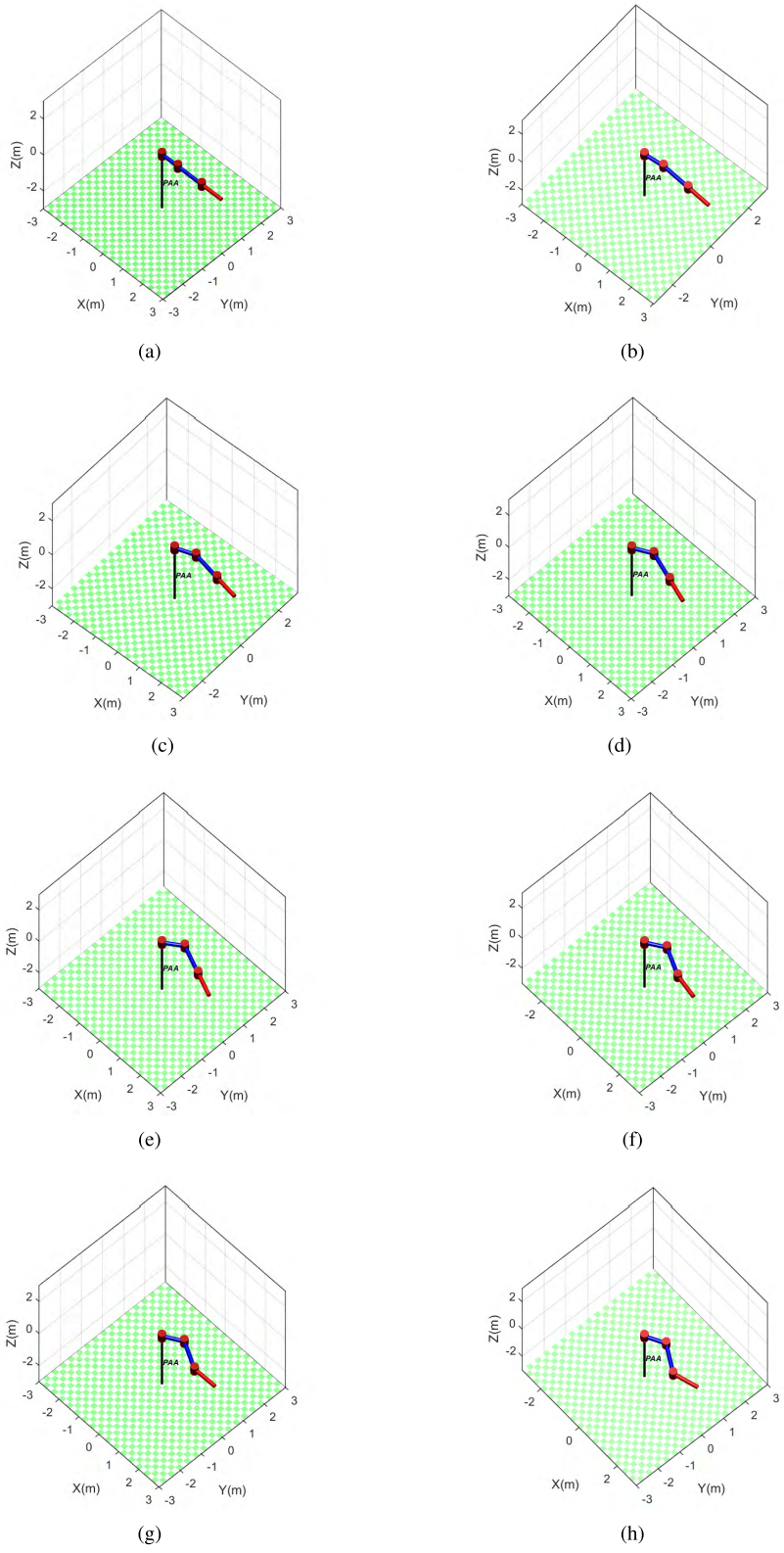

FIGURE 4. The motion state of the planar manipulator.

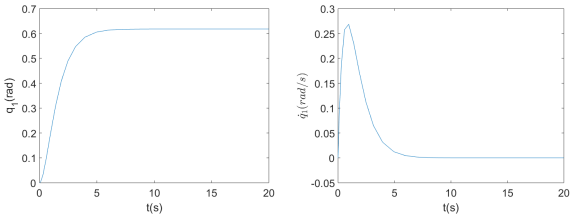

FIGURE 5. The angle and angular velocity curves of the first joint in the first stage.

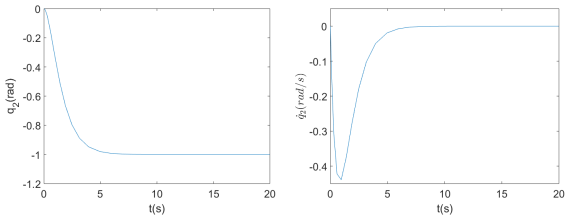

FIGURE 6. The angle and angular velocity curves of the second joint in the first stage.

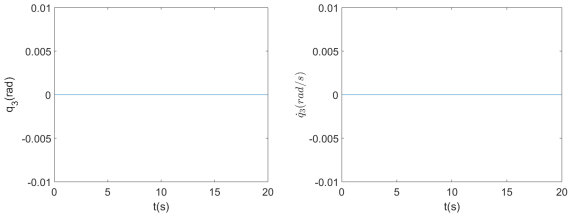

FIGURE 7. The angle and angular velocity curves of the third joint in the first stage.

TABLE 3. Parameters of the planar PAA under-actuated manipulator.

Link i	$m_i(kg)$	$L_i(m)$	$l_i(m)$	$J_i(kg \cdot m^2)$
$i=1$	0.8	0.8	0.4	0.04267
$i=2$	1.2	1.2	0.6	0.14400
$i=3$	1.0	1.0	0.5	0.08333

Then, the control law for the third joint can be obtained using

$$\tau_3 = \tau_{eq_2} + \tau_{sw2}. \tag{24}$$

Substituting equation (24) into equation (20), we can obtain the control law in the second stage

$$\begin{cases} \tau_2 = -(x_3 - x_3(0) + F_2(x) + c_2(x)\tau_3)/b_2(x) \\ \tau_3 = (b_2(x)(c_2x_6 + F_3(x) + w_2|S_2|^{\alpha_2}sgn(S_2)) \\ \quad -b_3(x)(x_3 - x_3(0) + F_2(x))) \\ \quad /(b_3(x)c_2(x) - b_2(x)c_3(x)). \end{cases} \tag{25}$$

Remark 2: τ_3 is proportional to the parameter w_2 and the steady-state adjustment time is inversely proportional to the parameter w_2. The parameter α_2 affects the smooth of the torque curve. If α_2 is selected too small, it will lead to oscillations of the torque curve.

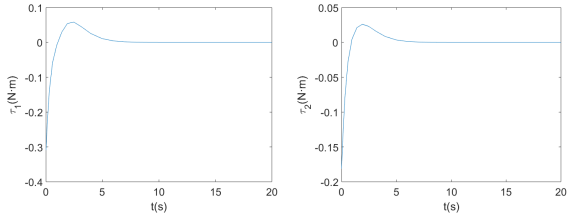

FIGURE 8. The torque curves of the active joints in the first stage.

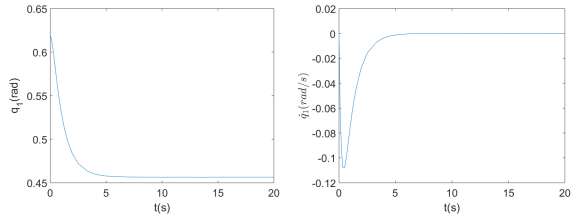

FIGURE 9. The angle and angular velocity curves of the first joint in the second stage.

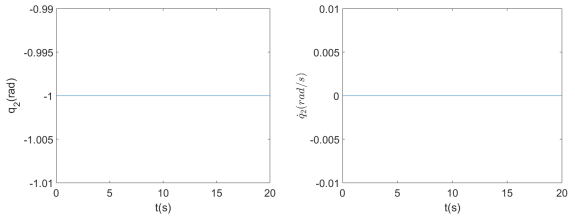

FIGURE 10. The angle and angular velocity curves of the second joint in the second stage.

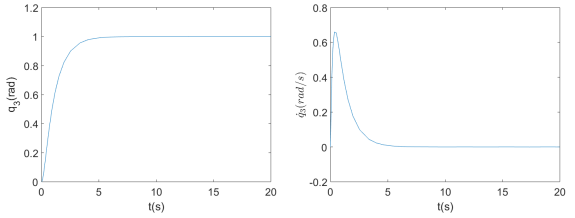

FIGURE 11. The angle and angular velocity curves of the third joint in the second stage.

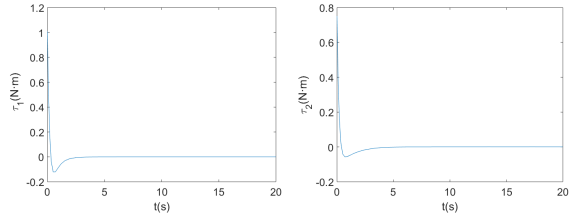

FIGURE 12. The torque curves of the active joints in the second stage.

C. STABILITY ANALYSIS

In this section, we analyze the stability of the designed control laws (17) and (25). In first stage, under the premise that the control law (12) is designed to maintain the angle of the

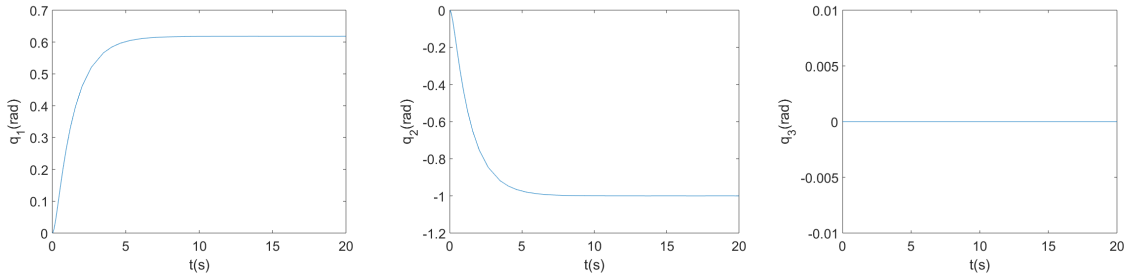

FIGURE 13. The angle curves of the joints in the first stage.

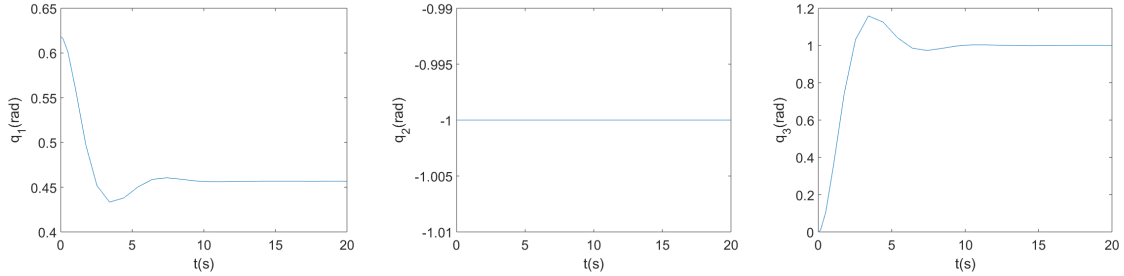

FIGURE 14. The angle curves of the joints in the second stage.

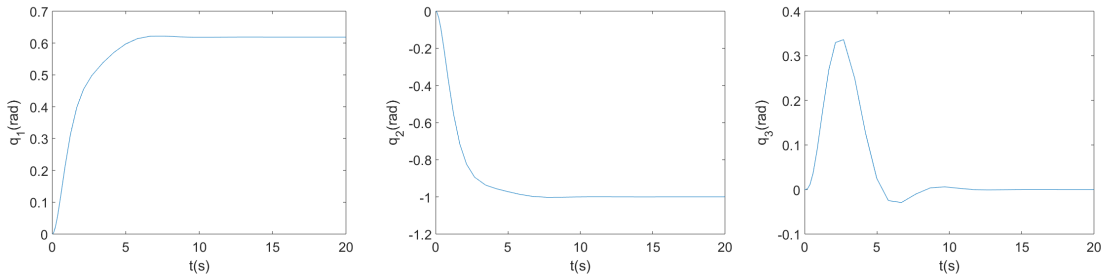

FIGURE 15. The angle curves of the joints in the first stage.

third joint unchanged, the PAA under-actuated manipulator is equivalent to a PA under-actuated manipulator. If the control law (16) can stabilize the PA under-actuated manipulator, the PAA under-actuated manipulator will be stable in Lyapunov sense.

Consider the following Lyapunov function candidate

$$V_3 = {S_1}^2/2. \tag{26}$$

Take its time derivative

$$\begin{aligned}\dot{V}_3 &= S_1\dot{S}_1 \\ &= S_1(c_1x_4 + F_2(x) + b_2(x)\tau_2 + c_2(x)\tau_3) \\ &= S_1(c_1x_4 + F_2(x) + b_2(x)(\tau_{eq1} + \tau_{sw1}) + c_2(x)\tau_3) \\ &= S_1b_2(x)\tau_{sw1} \\ &= -w_1{S_1}^2 \le 0\end{aligned} \tag{27}$$

The equation (27) indicates that the designed control law in the first stage is stable in Lyapunov sense. We can also prove that the control law designed in the second stage is stable in Lyapunov sense in the same way.

V. SIMULATIONS

In the section IV, we design the control laws (17) and (25) by the two-stage switching hybrid control method. In this section, the simulations are conducted by MATLAB. The parameters of the manipulator are shown in Table 3.

The initial state of the manipulator, the target position of the end effector and the target angles of each active joint are as follows:

$$\begin{aligned} q_{10} &= q_{20} = q_{30} = 0, \\ \dot{q}_{10} &= \dot{q}_{20} = \dot{q}_{30} = 0(rad/s), \\ (X_d, Y_d) &= (2.6428, 0.1728), \\ q_{2d} &= -1(rad), \quad q_{3d} = 1(rad). \end{aligned}$$

A model of the planar PAA manipulator is built by the robotic toolbox in MATLAB. The motion of the manipulator from the initial position to the target position is shown in Fig. 4.

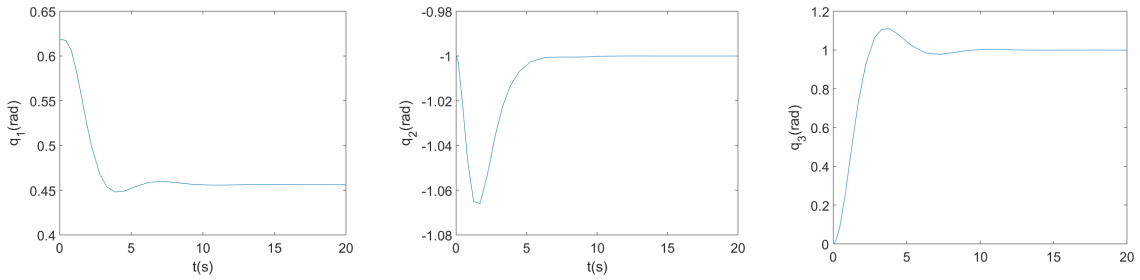

FIGURE 16. The angle curves of the joints in the second stage.

TABLE 4. Steady-state time and overshoot of the proposed control method.

Target angles(rad)	[1.08,-2,1]	[0.46,-1,1]	[-0.43,0.5,1]	[-0.47,0.5,2]
Overshoot of the second joint in the first stage	0%	0%	0%	0%
Steady-state time in the first stage	5.6s	5.5s	4.8s	4.8s
Overshoot of the second joint in the second stage	0%	0%	0%	0%
Steady-state time in the second stage	6.3s	7s	6.3s	7.4s

TABLE 5. Steady-state time and overshoot of the control method in [11].

Target angles(rad)	[1.08,-2,1]	[0.46,-1,1]	[-0.43,0.5,1]	[-0.47,0.5,2]
Overshoot of the second joint in the first stage	15%	15.8%	7.8%	7.8%
Steady-state time in the first stage	10.9s	15.3s	12.9s	12.9s
Overshoot of the second joint in the second stage	15.9%	15.9%	15.9%	15%
Steady-state time in the second stage	10.4s	12.4s	10.4s	9.8s

TABLE 6. Steady-state time and overshoot of the control method in [13].

Target angles(rad)	[1.08,-2,1]	[0.46,-1,1]	[-0.43,0.5,1]	[-0.47,0.5,2]
Overshoot of the second joint in the first stage	0%	0%	0%	0%
Steady-state time in the first stage	10.4s	13.6s	13.2s	13.2s
Overshoot of the second joint in the second stage	12.7%	11%	7.4%	5%
Steady-state time in the second stage	11.3s	10.2s	9s	9.6s

Fig 4(a)-Fig 4(d) show the motion state of the planar manipulator in the first stage where the third joint angle is unchanged and the second joint converges to its target angle. Fig 4(e)-Fig 4(h) show the motion state of the planar manipulator in the second stage where the second joint angle is unchanged and the third joint converges to its target angle.

The simulation results in Fig 4 show that the joint angle of each joint converges to its target angle very smoothly, and the end effector stabilizes at the target position.

The controller parameters are set as follows:

$$\begin{aligned} c_1 &= 5, \quad c_2 = 5, \\ w_1 &= 1.5, \quad w_2 = 1, \\ \alpha_1 &= 0.5, \quad \alpha_2 = 0.5. \end{aligned}$$

The first stage simulation curves are shown in Fig 5-8.

The control law switches to the second stage when the error between the actual joint angle and the target angle is less than 0.001. The second stage simulation curves are shown in Fig. 9-12.

Fig 5-12 illustrate the angle and the angular velocity of the third joint remain zero approximately while the second joint converges to the target angle in the first stage. In the second stage, the joint angle and the angular velocity of the second joint remain zero approximately while the third joint converges to the target angle.

Fig 13-14 and Fig 15-16 show the simulation curves of the manipulator controlled by the methods in [11] and [13], respectively.

According to the simulation results, the steady-state time of the proposed method is between 5s and 10s while the steady-state time of the methods in [11] and [13] are between 9s and 15s. The instance demonstrates that the control law realizes position control in a limited time and has obvious advantage in rapidity. What's more, we conduct more comparative simulations to verify the conclusion further. The simulation results are shown in Table 4, 5 and 6.

Table 4, 5 and 6 show the proposed method has shorter steady-state time than that of existing typical control methods, and its overshoot is almost zero.

VI. CONCLUSION

Based on the improved PSO algorithm, this paper presents a two-stage switching hybrid control method to realize the

position control of the planar three-link PAA under-actuated manipulator. The improved PSO introduces the Metropolis criterion of simulated annealing algorithm and the crowding factor of artificial fish swarm algorithm to increase the diversity of the particles, which reduces the probability of falling into local optimum. Therefore, the optimal target angles can be obtained. The two-stage switching hybrid control method guarantees an active joint angle unchanged by Lyapunov direct method and the other active joint converges to the target angle by sliding mode control. The proposed control method can be applied when the free swing fault happens. The free swing fault refers to the output torque of certain joint becomes to 0 and the friction influence of the passive joint can be neglected. The proposed method not only retains the rapidity of sliding mode control, but also reduces the total chattering of the system by Lyapunov function method. It also realizes the position control with shorter steady-state time than that of most existing typical control methods, and its overshoot is almost 0.

REFERENCES

[1] C. Qian and W. Lin, "A continuous feedback approach to global strong stabilization of nonlinear systems," *IEEE Trans. Autom. Control*, vol. 46, no. 7, pp. 1061–1079, Jul. 2001.

[2] V. Putranti and Z. H. Ismail, "Robust-save energy controller on an autonomous underwater vehicle with obstacles avoidance," in *Proc. IEEE Int. Conf. Underwater Syst. Technol., Theory Appl. (USYS)*, Penang, Malaysia, Dec. 2016, pp. 42–47.

[3] G. Mamakoukas, M. A. MacIver, and T. D. Murphey, "Feedback synthesis for underactuated systems using sequential second-order needle variations," *Int. J. Robot. Res.*, vol. 37, nos. 13–14, pp. 1826–1853, Apr. 2018.

[4] W. Sun, W.-X. Yuan, and Y.-Q. Wu, "Adaptive tracking control of mobile manipulators with affine constraints and under-actuated joints," *Int. J. Automat. Comput.*, vol. 15, no. 6, pp. 728–735, 2018.

[5] T. Yang, N. Sun, H. Chen, and Y. Fang, "Motion trajectory-based transportation control for 3-D boom cranes: Analysis, design, and experiments," *IEEE Trans. Ind. Electron.*, vol. 66, no. 5, pp. 3636–3646, May 2019.

[6] Z. Lin, Q.-D. Zhu, and Z.-Y. Xing, "Hierarchical sliding mode control for horizontal underactuated manipulators with optimization based on GA," *Control Decis.*, vol. 23, no. 1, pp. 99–102, 2008.

[7] A. D. Luca, R. Mattone, and G. Oriolo, "Stabilization of an underactuated planar 2R manipulator," *Int. J. Robust Nonlinear Control, IFAC-Affiliated J.*, vol. 10, no. 4, pp. 181–198, 2000.

[8] G. Oriolo and Y. Nakamura, "Control of mechanical systems with second-order nonholonomic constraints: Underactuated manipulators," in *Proc. 30th IEEE Conf. Decis. Control*, Brighton, U.K., Dec. 1991, pp. 2398–2403.

[9] A. D. Mahindrakar and R. N. Banavar, "Controllability properties of a planar 3R underactuated manipulator," in *Proc. Int. Conf. Control Appl.* Glasgow, U.K., Sep. 2002, pp. 489–494.

[10] Y. Sheng, X. Z. Lai, and M. Wu, "Position control of a planar three-link underactuated mechanical system based on model reduction," *Acta Autom. Sinica*, vol. 40, no. 7, pp. 1303–1310, Jul. 2014.

[11] X. Lai, Y. Wang, M. Wu, and W. Cao, "Stable control strategy for planar three-link underactuated mechanical system," *IEEE/ASME Trans. Mechatronics*, vol. 21, no. 3, pp. 1345–1356, Jun. 2016.

[12] R. A. DeCarlo, M. S. Branicky, S. Pettersson, and B. Lennartson, "Perspectives and results on the stability and stabilizability of hybrid systems," *Proc. IEEE*, vol. 88, no. 7, pp. 1069–1082, Jul. 2000.

[13] S. U. Din, Q. Khan, U.-R. Fazal, and R. Akmeliawanti, "A comparative experimental study of robust sliding mode control strategies for underactuated systems," *IEEE Access*, vol. 5, pp. 10068–10080, 2017.

[14] P.-Y. Xiong, X.-Z. Lai, and M. Wu, "Position and posture control for a class of second-order nonholonomic underactuated mechanical system," *IMA J. Math. Control Inf.*, vol. 35, no. 2, pp. 523–533, Sep. 2016.

[15] R. Köker, "A genetic algorithm approach to a neural-network-based inverse kinematics solution of robotic manipulators based on error minimization," *Inf. Sci.*, vol. 222, pp. 528–543, Feb. 2013.

[16] R. Köker, "A neuro-simulated annealing approach to the inverse kinematics solution of redundant robotic manipulators," *Eng. Comput.*, vol. 29, no. 4, pp. 507–515, Oct. 2013.

[17] X. Wu and Z. Xie, "Forward kinematics analysis of a novel 3-DOF parallel manipulator," *Scientia Iranica Trans. B, Mech. Eng.*, vol. 26, no. 1, pp. 346–357, 2019.

[18] M. Ayyildiz and K. Çetinkaya, "Comparison of four different heuristic optimization algorithms for the inverse kinematics solution of a real 4-DOF serial robot manipulator," *Neural Comput. Appl.*, vol. 27, no. 4, pp. 825–836, May 2016.

[19] T.-Y. Chen and T.-M. Chi, "On the improvements of the particle swarm optimization algorithm," *Adv. Eng. Softw.*, vol. 41, no. 2, pp. 229–239, 2010.

[20] M. Zambrano-Bigiarini, M. Clerc, and R. Rojas, "Standard particle swarm optimisation 2011 at CEC-2013: A baseline for future PSO improvements," in *Proc. IEEE Congr. Evol. Comput.*, Cancun, Mexico, Jun. 2013, pp. 2337–2344.

[21] M. A. Tolba, V. N. Tulsky, and A. A. Z. Diab, "Optimal sitting and sizing of renewable distributed generations in distribution networks using a hybrid PSOGSA optimization algorithm," in *Proc. IEEE Int. Conf. Environ. Elect. Eng. IEEE Ind. Commercial Power Syst. Eur.*, Milan, Italy, Jun. 2017, pp. 1–7.

[22] Y. Wang, X. Lai, L. Chen, H. Ding, and M. Wu, "A quick control strategy based on hybrid intelligent optimization algorithm for planar n-link underactuated manipulators," *Inf. Sci.*, vol. 420, pp. 148–158, Dec. 2017.

[23] B. Gao, X. Zhang, H. Chen, and J. Zhao, "Energy-based control design of an underactuated 2-dimensional TORA system," in *Proc. IEEE/RSJ Int. Conf. Intell. Robots Syst.*, St Louis, MO, USA, Oct. 2009, pp. 1296–1301.

[24] S. Lyden and M. E. Haque, "A simulated annealing global maximum power point tracking approach for PV modules under partial shading conditions," *IEEE Trans. Power Electron.*, vol. 31, no. 6, pp. 4171–4181, Jun. 2016.

[25] C. Jiang, L. Wan, Y. Sun, and Y. Li, "The application of PSO-AFSA method in parameter optimization for underactuated autonomous underwater vehicle control," *Math. Problems Eng.*, vol. 2017, Aug. 2017, Art. no. 6327482.

[26] A. G. Filippov, "Application of the theory of differential equations with discontinuous right-hand sides to non-linear problems in automatic control," *IFAC Proc. Vol.*, vol. 1, no. 1, pp. 933–937, 1960.

XIN GAO received the B.S. degree in control science and engineering from North China University of Technology, Beijing, China, in 1997, the M.S. degree in pattern recognition and intelligent system from Beijing University of Technology, China, in 2002, and the Ph.D degree from the Beijing University of Aeronautics and Astronautics, in 2007. From 2011 to 2014, he is the Executive Deputy Director of Automation Teaching and Research Centre at the Beijing University of Posts and Telecommunications. He is currently an Associate Professor of Department of Automation. His research interests include space robotics, virtual reality technology, intelligent systems, etc. He has published over 30 refereed journal papers and conference papers, and holds more than 20 patents.

ZEYU REN received the B.S. degree from the Beijing University of Posts and Telecommunications, China, in 2017. He is currently pursuing the master's degree with the Beijing University of Posts and Telecommunications, China. His research interests include space robotics and robot control.

LIN ZHAI received the B.S. degree from the Beijing University of Posts and Telecommunications, China, in 2016. He is currently pursuing a master's degree with the Beijing University of Posts and Telecommunications, China. His research interests include space robotics and robot control.

QINGXUAN JIA (M'09) received the B.S. and M.S. degrees in mechanical engineering from the Shandong University of Technology, Shandong, China, in 1988 and 1991, respectively. And he received the Ph.D. degree in electromechanical engineering and automation from the Beijing University of Aeronautics and Astronautics, Beijing, China, in 2005. He is the Professor with the School of Automation, Beijing University of Posts and Telecommunications. His research interests include space robotics, virtual reality technology, and pattern recognition.

HUIHE LIU received the B.S. degree from the Beijing University of Posts and Telecommunications, China, in 2017. He is currently pursuing a master's degree with the Beijing University of Posts and Telecommunications, China. His research interests include space robotics and deep learning.